

TUTORIAL • OPEN ACCESS

## Fiber-optics based fluorescence detection. Part I: Basic concepts

To cite this article: Bong Lee *et al* 2024 *Methods Appl. Fluoresc.* **12** 043001

View the [article online](#) for updates and enhancements.

### You may also like

- [On the origin and correction for inner filter effects in fluorescence Part I: primary inner filter effect-the proper approach for sample absorbance correction](#)  
Joseph Kimball, Jose Chavez, Luca Ceresa et al.
- [A simple light path modifying device to reduce scattering in front-face fluorescence spectra](#)  
Frank B Peters and Andreas O Rapp
- [A review on fluorescence spectroscopic analysis of water and wastewater](#)  
Muhammad Farooq Saleem Khan, Mona Akbar, Jing Wu et al.

# Methods and Applications in Fluorescence



## TUTORIAL

# Fiber-optics based fluorescence detection. Part I: Basic concepts

### OPEN ACCESS

RECEIVED  
15 January 2024

REVISED  
10 June 2024

ACCEPTED FOR PUBLICATION  
2 July 2024

PUBLISHED  
23 July 2024

Bong Lee<sup>1</sup>, Luca Ceresa<sup>1</sup>, Danh Pham<sup>1</sup>, Joseph Kimball<sup>1</sup>, Emma Alexander<sup>1</sup>, Xuan Ye<sup>2</sup>, Ignacy Gryczynski<sup>1</sup> and Zygmunt Gryczynski<sup>1</sup>

<sup>1</sup> Department of Physics and Astronomy, Texas Christian University, Fort Worth, TX, 76109, United States of America

<sup>2</sup> Organometallic Catalysis, Novel Products Research, ExxonMobil Technology and Engineering Company, Baytown, TX, 77520, United States of America

E-mail: [bong.lee@tcu.edu](mailto:bong.lee@tcu.edu)

**Keywords:** spectroscopy, fiber optic, fluorescence, absorption, inner filter effect

Original content from this work may be used under the terms of the [Creative Commons Attribution 4.0 licence](https://creativecommons.org/licenses/by/4.0/).

Any further distribution of this work must maintain attribution to the author(s) and the title of the work, journal citation and DOI.



## Abstract

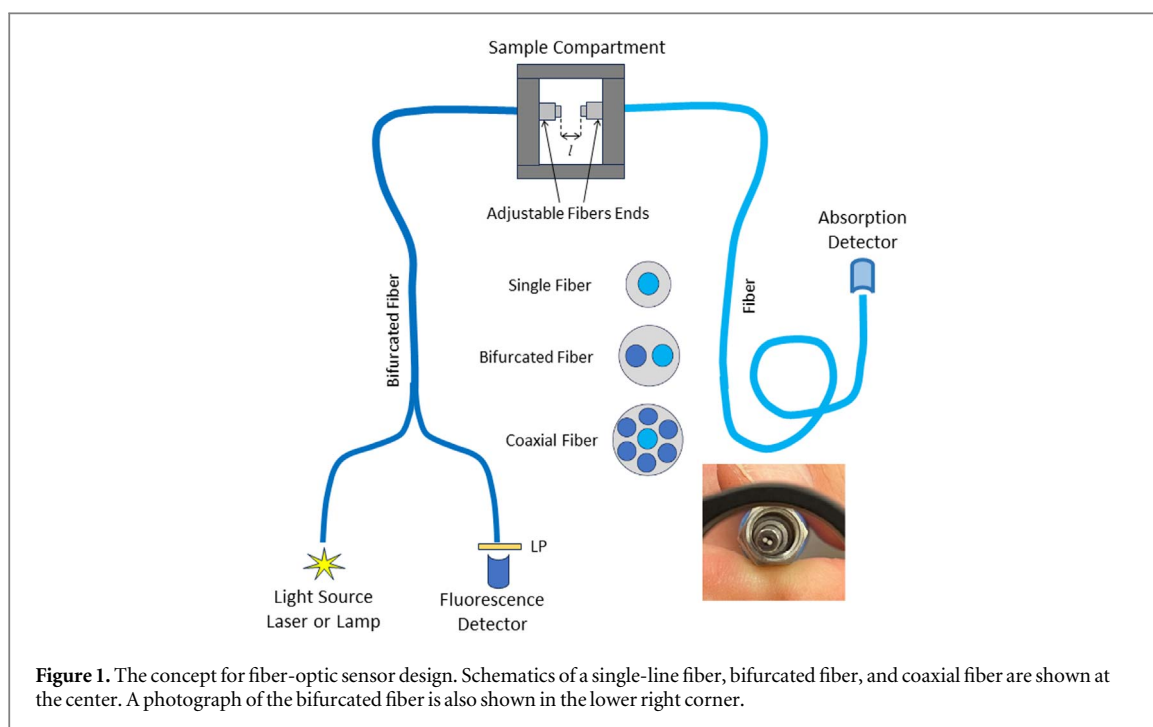
Continuous in-line detection and process monitoring are essential for industrial, analytical, and biomedical applications. Lightweight, highly flexible, and low-cost fiber optics enable the construction of compact and robust handheld devices for *in situ* chemical and biological species analysis in both industrial and biomedical *in vitro/in vivo* detection. Despite the broad range of fiber-optic based applications, we lack a good understanding of the parameters that govern the efficiency of light collection or the sensitivity of detection. Consequently, comparing samples of different optical density and/or geometry becomes challenging and can lead to misinterpretation of results; especially when we lack the approaches necessary to correct the detected signal (spectra) for artifacts such as inner-filter effect or scattering. Hence, in this work, we discuss factors affecting the signal detected by the fiber optic in the bare and lens-coupled flat-tipped configurations that lead to signal/spectral distortions. We also present a simple generic model describing the excitation profile and emission collection efficiency that we verify with experimental data. Understanding the principles governing the signal collected by the fiber will provide rationales for correcting the measured emission spectra and recovering the true emission profile of optically dense samples.

## 1. Introduction

Fiber-optic based detection enables various remote applications ranging from analytical sciences, remote sensing, industrial applications, monitoring physico-chemical processes, and chemical species analysis [1–10]. They enable optical spectroscopy (absorption, fluorescence, or Raman) to be performed on inaccessible sites through conventional spectroscopic instrumentation. Most applications are limited to ratiometric-type detection [7, 11–15] or overall intensity detection.

Fiber-optics based fluorescence applications typically use a bifurcated fiber probe or its improved version, a coaxial fiber probe [7, 12–18]. An example of a bifurcated/coaxial fiber arrangement is shown in figure 1. With such a fiber, various probe architectures can be constructed easily without the use of sophisticated setups incorporating extra filters and/or mirrors. This type of arrangement has also been shown to be convenient for the detection of weak

(low quantum yield) fluorophores [18]. Most fiber applications use optically thin detection sensors at the end of the fiber tip or are used for collecting fluorescence emissions from low optical density samples, where the inner-filter effect or geometrical factors are negligible [19–23]. For example, we were unable to find reports on practical applications for fiber-optic probes, where samples with high optical density would require correcting for the inner filter effect. However, emerging practical applications of fiber optics in the chemical industry or biomedical diagnostics frequently use optically dense samples for which significant variability in sample optical density, transparency, or scattering is expected. Comparing the results (e.g. emission spectra modification or intensity changes) from such samples without proper correction could be challenging or even misleading [19]. Such correction procedures for fluorescence signals measured in classic square geometry systems are now well understood and applied [21, 24]. However, a proper correction for



measurements in front-face configurations is much more complex [21, 24], and corrections for fiber-optics detections are practically not used/developed at all. Given the rapidly growing popularity of fiber-optics based detection, we anticipate that many practical applications will benefit from such a correction, enabling more analytical uses.

In this report, we investigated the use of the flat-tipped coaxial fiber-optic probe to detect the fluorescence signal from samples with low and high optical density in different thickness layers up to bulk sample solutions (unlimited thickness). We considered a bare flat-tipped fiber and one equipped with a collimating lens. We found that the efficiency of detected emission by bare fiber highly depends on the distance and sample thickness, making it difficult to apply an appropriate correction for the sample's inner filter effect. In contrast, by using a collimating lens, the efficiency for detecting the emission signal does not depend on distance within a large range (up to  $\sim 20$  mm). Based on these findings, we propose a simple and robust fiber-optic probe design that can be used for simultaneous measurements of sample absorption and fluorescence. In Part I, we present theoretical considerations with experimental verifications for distance-dependent efficiency of detected fluorescence signal by a bare fiber end and a fiber equipped with a collimating lens. We test absorption measurements using a fiber optic system and compare them to absorption measured by commercial instruments. Finally, we present model experiments demonstrating spectra distortion for high optical density samples due to the inner filter effect. A practical approach to correct measured emission spectra for the inner filter effect, yielding a true

unperturbed emission spectrum for different chromophores, will be discussed in Part II.

### 1.1. General concept

In the following discussion, we present a simplified description of concepts for a fiber-optic probe design. The emission spectra measured from bulk samples with significant absorption will be affected by multiple factors related to the sample specification or geometrical/optical factors of the probe. To properly interpret the observed emission spectra, it will be necessary to correct the measurement for multiple factors like the geometry of the excitation beam emerging from the fiber, distance-dependent efficiency for signal collection, and inner filter effect. To correctly account for all these factors, we present a simple theoretical model and provide a set of experiments to measure the absorption and emission of samples of different thicknesses and optical densities.

A schematic concept for the fiber-optics sensor is presented in figure 1. The sample compartment is equipped with two opposite-facing fiber optics. The distance (separation,  $l$ ) between fibers can be adjusted adequately for a given sample's absorption. Mounted on the left side of the sample compartment is the end of the bifurcated fiber-optic cable that delivers excitation light for fluorescence or white light (or variable wavelength light) for absorption measurements. The second line of the bifurcated fiber-optic cable collects the fluorescence emission signal. This detection side is equipped with a long pass (LP) filter to reject scattered excitation light. In principle, a single-line fiber-optic cable can be used on the left side, but an appropriate dichroic filter has to be used for coupling the

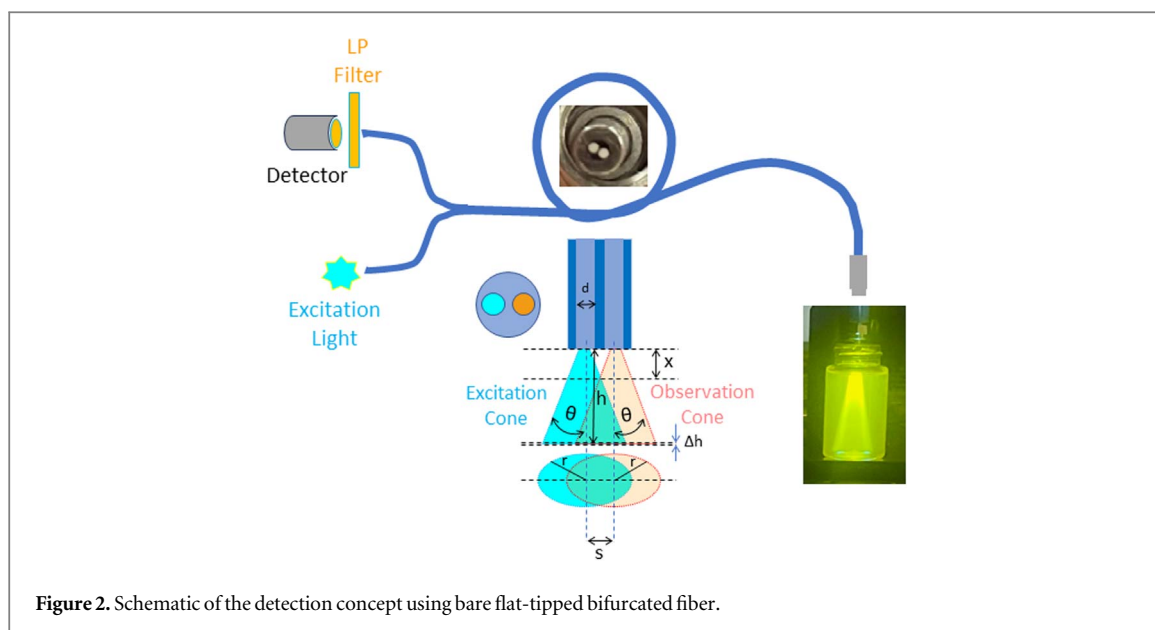


Figure 2. Schematic of the detection concept using bare flat-tipped bifurcated fiber.

excitation and selecting the emission light. Such configuration for emission measurements is equivalent to a front face in-line configuration discussed by us earlier [19, 21, 24].

On the right side of the sample compartment, a single-line fiber-optic cable is mounted; it can also be a bifurcated fiber, but for simplicity of this description we consider an ordinary single-line fiber. The fiber collects the light transmitted through the sample and delivers the light to a detector (e.g., Ocean Optics) capable of measuring wavelength-dependent transmitted light intensity. When compared with the light intensity measured from a reference sample/solvent, the sample absorption can be calculated. This detection line can also be used to monitor fluorescence emission signal when equipped with an appropriate filter. Thus, in the presented configuration, we can measure emission and absorption simultaneously or in a repeating sequence. The measured absorption can/will be used later to correct measured emission spectra for inner filter effects.

In the following sections, we will discuss the potential use of fiber optics without the collimating optics (bare flat-tipped fiber) and fiber optics equipped with a collimating optical element/lens. We will discuss the use of a bifurcated fiber for light delivery and emission collection that is easier to use in practice (no need for special dichroic filters and excitation light coupling) and is commonly applied. But we want to stress that the presented model directly applies to coaxial fibers and can be adapted to single-line fibers. A single-line fiber can be considered as a version of bifurcated fiber, where both lines perfectly overlap but the coupling of excitation light and separation of emission light will require a more advanced optical filtering system. Both configurations, bare fiber and fiber equipped with a lens, can be used for measuring the emission of chemical/biological materials directly, in

closed containers (bottles, chemical reactor chambers, in a flow-cell integrated into the chemical reactor), or in biological applications for measuring fluorescence on the skin or through the skin in tissue.

## 2. Bare fiber-optics detection

### 2.1. Bifurcated fiber

First, we consider a basic bifurcated fiber without lenses or additional optical elements. To calculate the fluorescent signal detected through a flat-tipped bifurcated/coaxial fiber probe, we considered the configuration shown in figure 2, a geometrical design originally discussed by Ma *et al* [18], where one of the arms of the bifurcated fiber delivers the excitation, and the other collects the emission signal. A long pass (LP) filter is placed on the detection side to block scattered and reflected excitation light. The lower part of figure 2 provides detailed information on the geometrical parameters for the excitation beam formed by the excitation line of the fiber and the observation area detected by the second line of the fiber. As presented in the photograph on the right side of figure 2, the light emerging from the fiber forms a cone described by the angle,  $\theta$ , measured relative to the fiber axis. The cone angle,  $\theta$ , directly relates to the fiber's numerical aperture (NA) that depends on the refractive index gradient between the core and cladding. For simplicity, we assumed that both branches of the fiber are identical, and the efficiency distribution of emission collected by the second fiber line forms an identical cone to the one formed by the excitation light. Both cones are separated by a distance  $s$ . At any distance,  $h$ , from the fiber tip, photons detected by a collecting fiber can only emerge from the overlapping area of both cones (the overlapping region between the two circles is marked in green). As calculated in [16, 18], the overlapping area between two circles is given by:

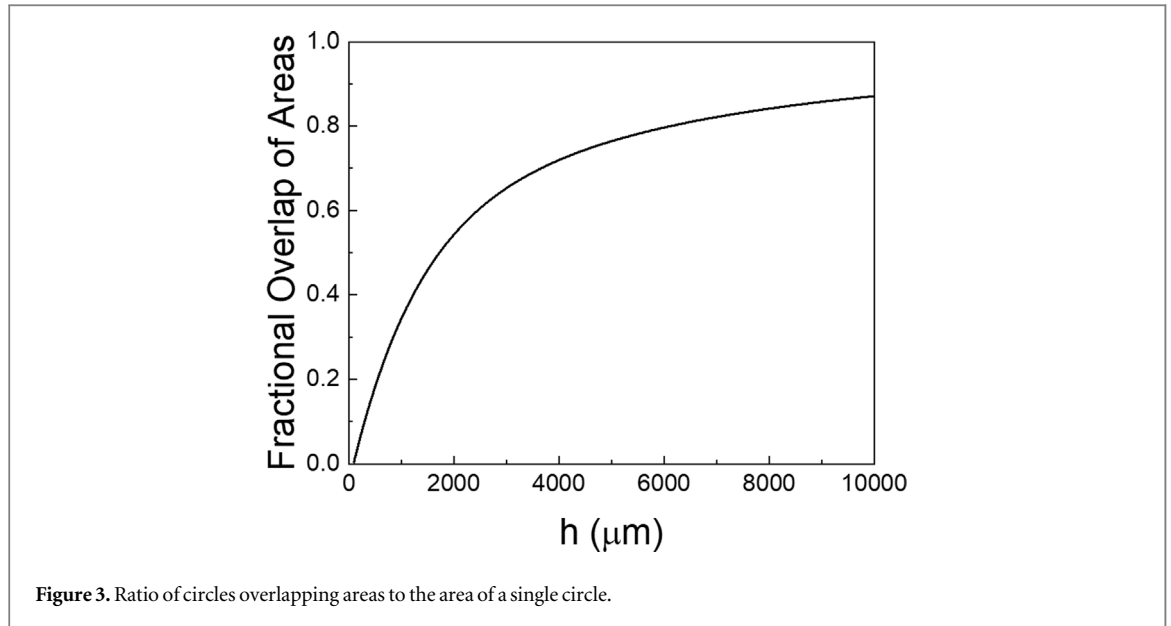


Figure 3. Ratio of circles overlapping areas to the area of a single circle.

$$\Delta S = 2 \left( r^2 \cos^{-1} \left( \frac{s}{2r} \right) - s \sqrt{r^2 - \left( \frac{s}{2} \right)^2} \right) \quad (1)$$

where the radius of the circle,  $r$ , is  $\frac{d}{2} + h \tan(\theta)$  and  $d$  is the diameter of the fiber.

Depending on the separation of the internal fiber lines,  $s$ , and angle,  $\theta$ , we have a distance,  $x$ , for which the overlap between the excitation and collection cones does not occur and we will not detect any emission signal. Only when the distance  $h$  is greater than  $x$  will the emission signal be detected. Also, the fraction of the overlapping area between both cones quickly increases with distance  $h$ . The surface area of each circle at a given distance  $h$  is given by  $S = \pi r^2$ . We can then define the ratio  $R = \frac{\Delta S}{S}$  which represents the fraction of the overlapping area relative to the area of a single circle. In figure 3, the ratio,  $R$ , is presented for an assumed fiber line diameter of  $600 \mu\text{m}$ , and the separation between the fiber lines centers is  $s = 900 \mu\text{m}$  (for this separation between centers, the distance between the two closest fiber edges is  $300 \mu\text{m}$  (50% of the fiber diameter)). The angle  $\theta$  was assumed to be  $12.5^\circ$  ( $2\theta = 25^\circ$ ). From figure 3, it is evident that up to about  $700 \mu\text{m}$ , we should not detect any signal. Up to this distance, the emission detection cone does not overlap with the excitation cone, and emission should not be observed. The overlapping area rapidly increases past this limit, and the ratio asymptotically approaches 1. This is expected since for when  $h \gg s$  the cones will completely overlap.

Assuming that the fiber touches or is in the sample as the light penetrates the sample, it is absorbed, and its intensity decreases according to the Beer-Lambert law:

$$I(h) = I_0 10^{-\varepsilon Ch} \quad (2)$$

where  $I_0$  is the initial excitation light intensity leaving the fiber,  $\varepsilon$  is the extinction coefficient,  $C$  is concentration, and  $h$  is distance. This is just an approximation valid for a small angle,  $\theta$ , where we can assume that the distance from the tip of the fiber to the center of the circle or edge of the circle is similar/comparable. Assuming that the excitation light intensity is uniformly distributed in the cone, the power density of excitation light in the circle cross-section of the cone (intensity per unit of surface,  $i$ ) at any distance  $h$  can be described as:

$$i(h) = \frac{I(h)}{\pi \left( \frac{d}{2} + h \tan(\theta) \right)^2} \quad (3)$$

The number of excited fluorophores in any thin layer,  $\Delta h$ , at distance  $h$  is proportional to the amount of light absorbed by the layer (see figure 2):

$$\Delta N \sim I(h)(1 - 10^{-\varepsilon C \Delta h}) = I_0 10^{-\varepsilon Ch} (1 - 10^{-\varepsilon C \Delta h}) \quad (4)$$

The fraction of excited fluorophores in the overlapping region of two circles is proportional to the overlapping area,  $R = \frac{\Delta S}{S}$ :

$$\Delta n = \Delta N \frac{\Delta S}{S} = I_0 10^{-\varepsilon Ch} (1 - 10^{-\varepsilon C \Delta h}) \frac{2r^2 \cos^{-1} \left( \frac{s}{2r} \right) - s \sqrt{r^2 - \left( \frac{s}{2} \right)^2}}{\pi \left( \frac{s}{2} + h \tan(\theta) \right)^2} \quad (5)$$

where  $\Delta n$  represents the fraction of excited fluorophores seen by the second fiber line from the layer  $\Delta h$  at distance  $h$ . To approximate the signal detected by the collecting fiber line, separated by a distance  $s$  from the excitation fiber line, we assume that  $h > s$  and angular displacement is negligible. As shown in figures 2 and 3, the distance for which the cones start

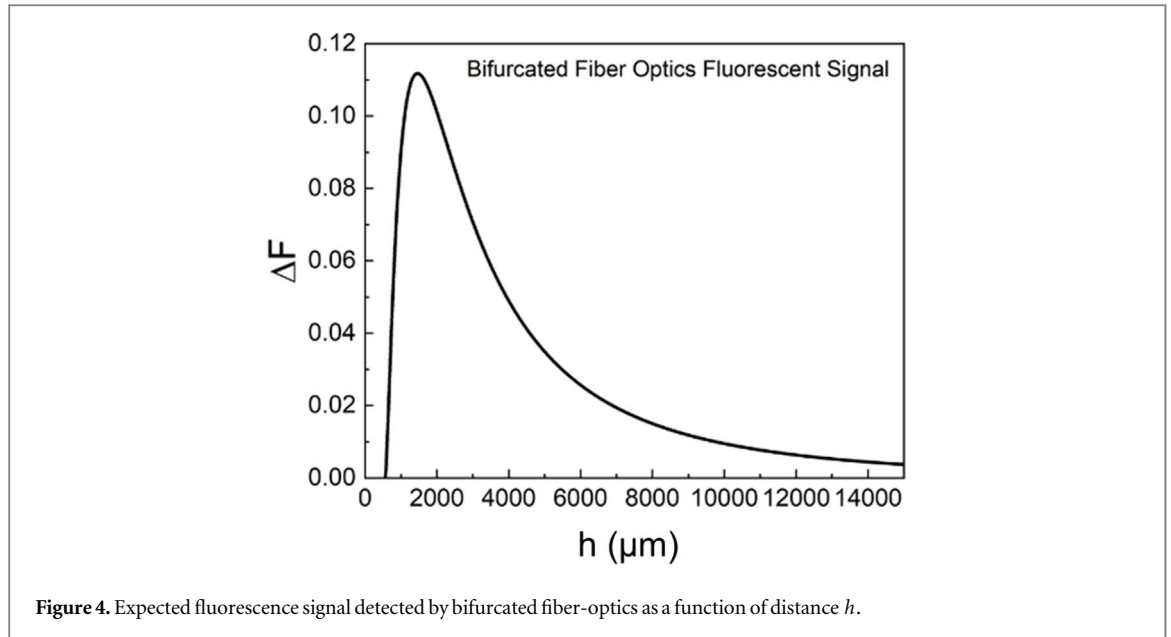


Figure 4. Expected fluorescence signal detected by bifurcated fiber-optics as a function of distance  $h$ .

overlapping (minimum distance for which we start detecting fluorescence) depends on distance  $s$  and angle  $\theta$ , and for small  $\theta$  is significant. Fluorophores emit randomly in all directions (uniform 3D emission distribution), so the emission fraction that will reach the detection fiber of diameter  $d$  for small angle  $\theta$  depends on distance  $h$  and can be approximated by:

$$t = 1 - \frac{\sqrt{h^2 - \left(\frac{d}{2}\right)^2}}{h} \quad (6)$$

The distance-dependent factor,  $t$ , represents the amount of light emitted toward the second fiber. As distance  $h$  increases, the detected emission fraction decreases. We can approximate the detected fluorescence signal,  $\Delta F$ , from an overlapping surface at any distance  $h$  as:

$$\begin{aligned} \Delta F_h &= \Delta n QY t \\ &= I_0 10^{-\varepsilon Ch} (1 - 10^{-\varepsilon C \Delta h}) \frac{2r^2 \cos^{-1}\left(\frac{s}{2r}\right) - s \sqrt{r^2 - \left(\frac{s}{2}\right)^2}}{\pi \left(\frac{s}{2} + h \tan(\theta)\right)^2} QY \left(1 - \frac{\sqrt{h^2 - \left(\frac{d}{2}\right)^2}}{h}\right) \end{aligned} \quad (7)$$

where the absorbance of a thin layer of the sample ( $\Delta h$ ) is  $\Delta A = \varepsilon C \Delta h$ , and  $QY$  is the quantum yield of a sample.

In our approximation, the probability of detecting a photon emerging from the left or right side of an overlapping area is the same. In fact, the efficiency of the detection (sensitivity) could be slightly different due to the difference in angle for various points on the overlapping region.

In figure 4, we present the theoretical dependence of the signal measured from a thin layer sample ( $\Delta A$ ) as a function of distance  $h$  using equation (7). Up to the distance  $x$ , we do not detect any signal (the excitation circle and observation circle do not overlap). From distance  $x$ , the detected signal quickly increases, reaching a maximum, and then drops.

As depicted in figure 4, the largest contribution to the observed emission will be from the initial layers, while deeper layers contribute less and less. This is because, for small distances, the signal growth is dominated by the increase of circles overlapping area, and, for larger distances, the signal change is driven by the factor  $t$  resulting in the distance dependent collection efficiency.

To test this prediction, we used the experimental arrangement shown in figure 5. To obtain a narrow

fluorescent layer of small absorbance,  $\Delta A$ , we produced a thin ( $\sim 100 \mu\text{m}$  thick) PVA film containing Rhodamine 6G (R6G). The film is placed in a petri dish (inset in figure 5) underneath the fiber-optics mounted on a precise positioner capable of moving up and down. The full turn of the positioner screw corresponds to  $500 \mu\text{m}$  displacement (2 turns per 1 mm). Figure 6 shows the measured emission signals from the R6G film as a function of the distance

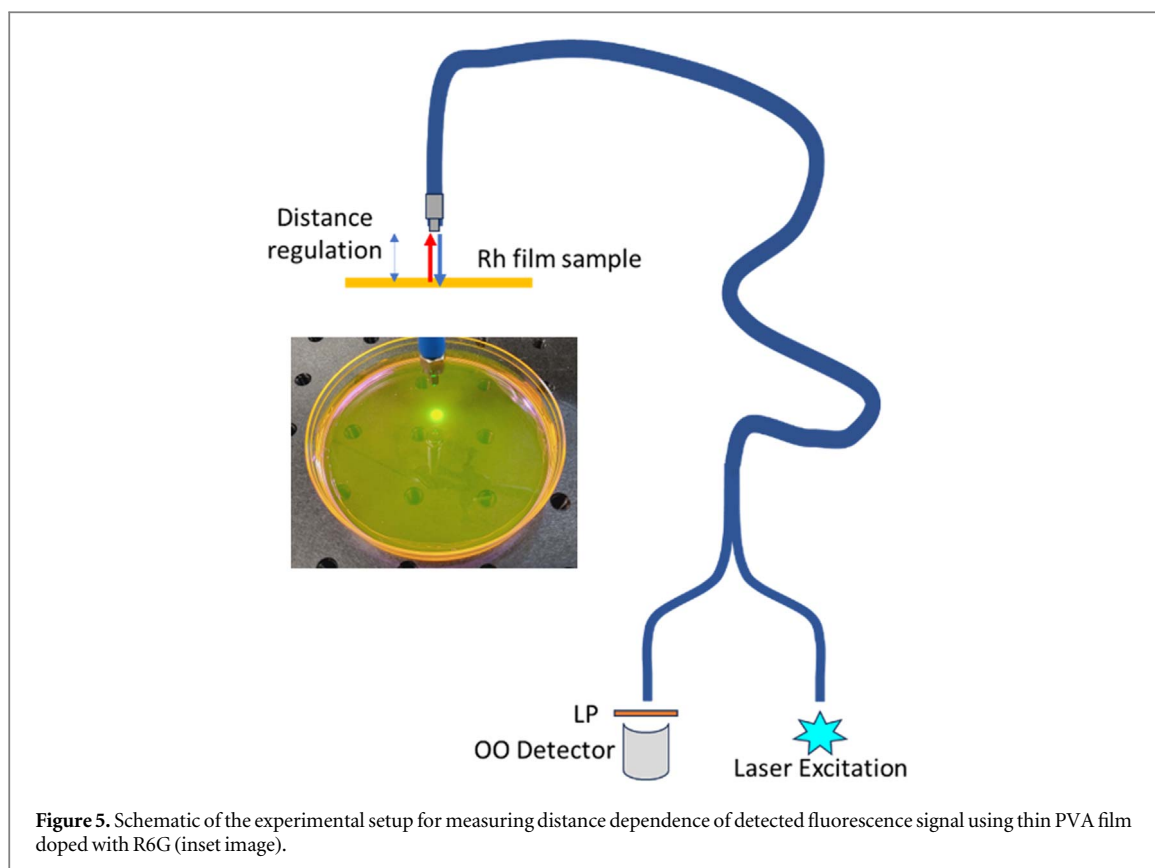


**Figure 5.** Schematic of the experimental setup for measuring distance dependence of detected fluorescence signal using thin PVA film doped with R6G (inset image).

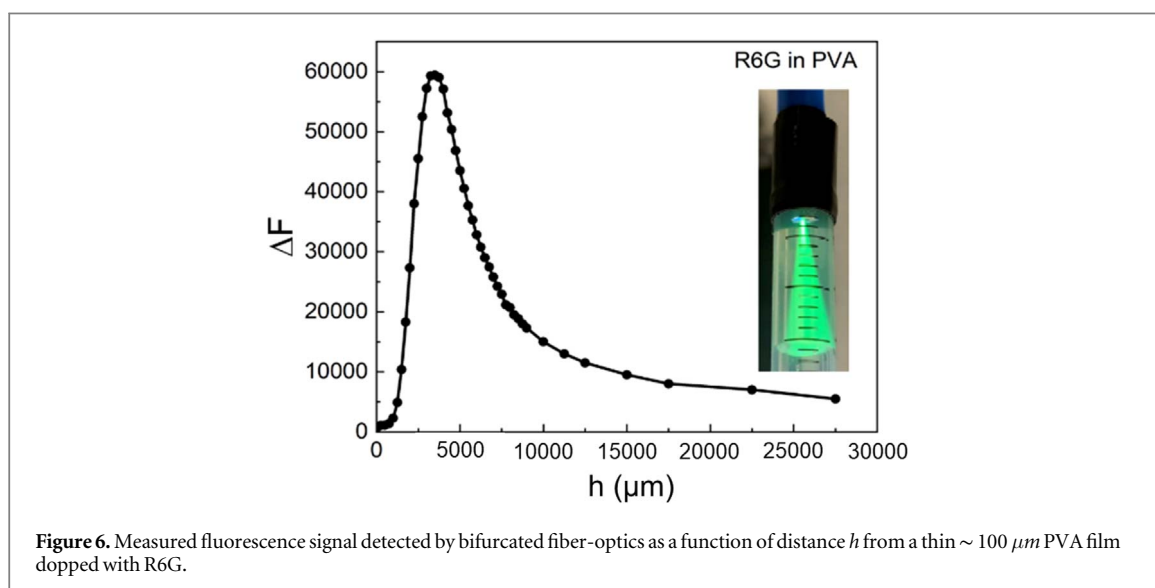
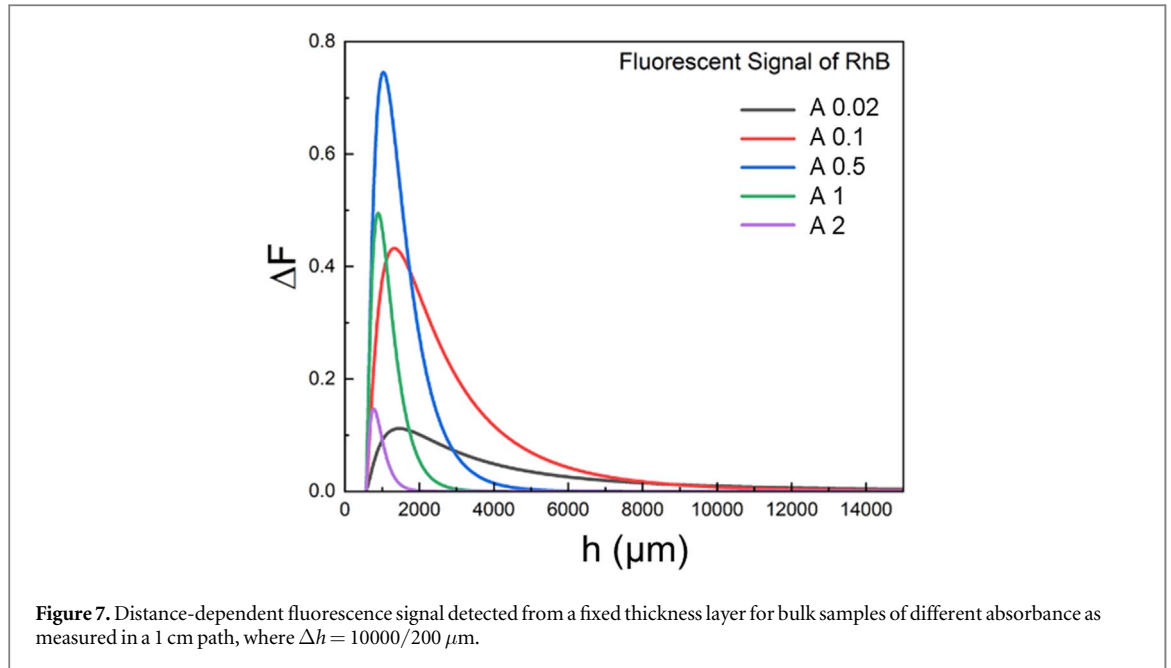


**Figure 6.** Measured fluorescence signal detected by bifurcated fiber-optics as a function of distance  $h$  from a thin  $\sim 100 \mu\text{m}$  PVA film doped with R6G.

between the film and the fiber-optic tip (as function of number of turns). The absorption of the film is below 0.05 ( $\Delta A < 0.05$ ), so we can neglect the inner filter effect [19, 22], while the emission signal with 480 nm excitation is high (easily detectable). For the first 2–3 steps, the fluorescence signal is very low. This small count, in the order of 1–2% of the maximum signal, is the result of fluorophores being excited by reflections and scattering of the excitation light on the film's surfaces and inside the film.

Overall, despite multiple approximations being made, the experimental results align well with our theoretical predictions.

It is interesting to consider a distance-dependent signal that will reach the detector from a bulk continuous solution of a given absorbance and thickness. The observed signal will depend on sample absorbance and distance-dependent light collection efficiency (geometrical factors). For the assumed bifurcated fiber parameters ( $d = 600 \mu\text{m}$  and separation of



$s = 900 \mu\text{m}$ ), the intensity detected from an  $i$ th thin layer of the thickness  $\Delta h$  that for a given  $i$  is at the distance/depth  $h_i = i\Delta h$  will be:

$$\Delta F_i = \Delta n_i QY f$$

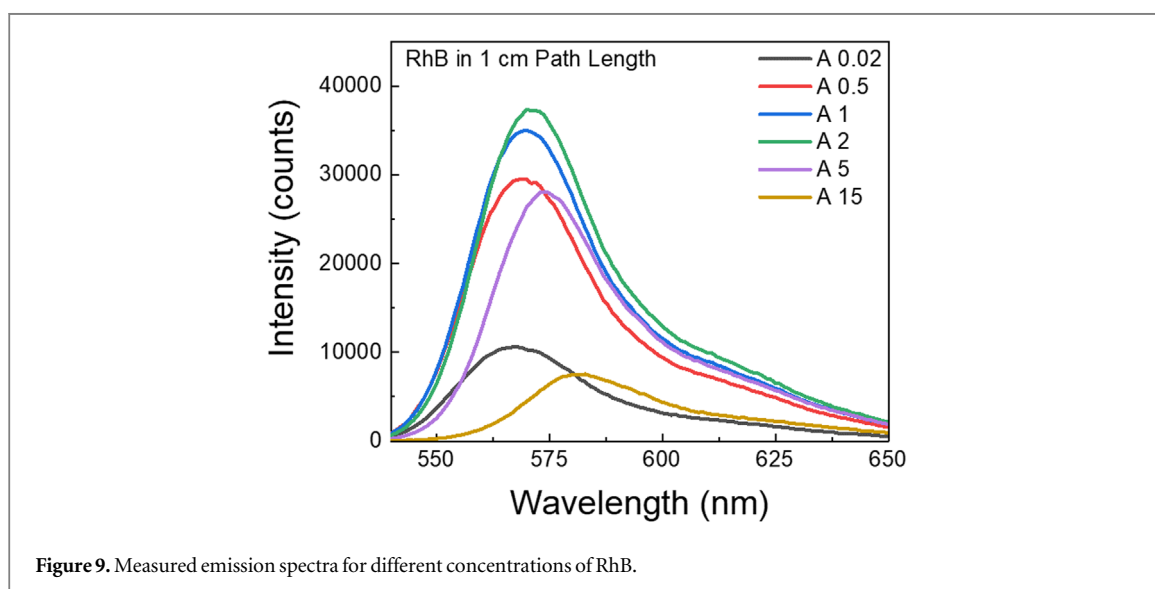
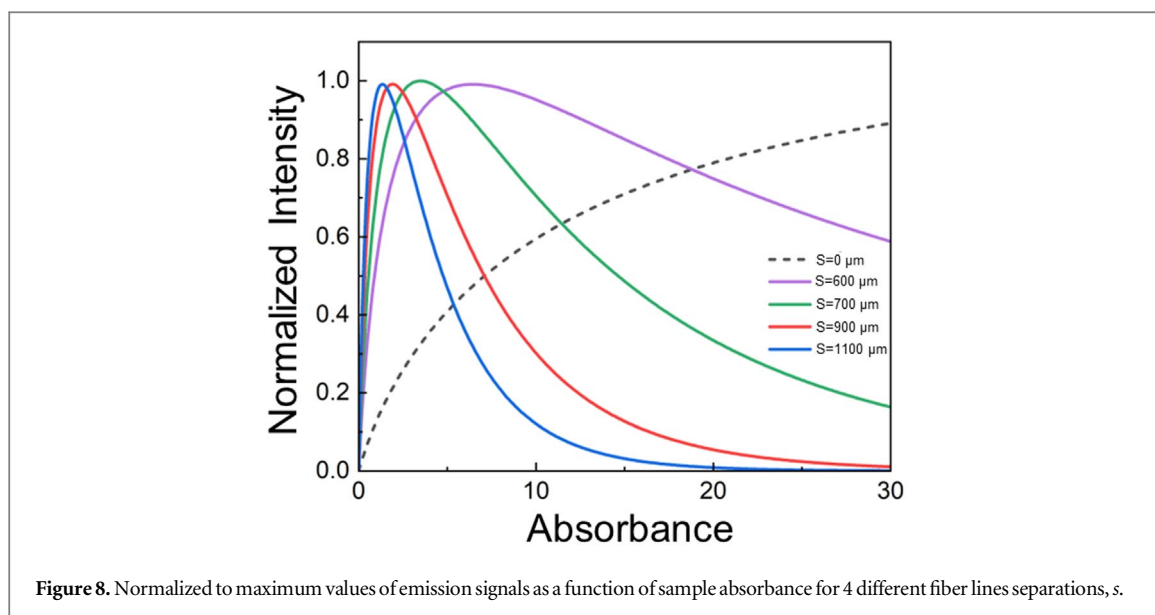
$$= I_0 10^{-\varepsilon C i \Delta h} (1 - 10^{-\varepsilon C \Delta h}) \frac{2r^2 \cos^{-1}\left(\frac{s}{2r}\right) - s \sqrt{r^2 - \left(\frac{s}{2}\right)^2}}{\pi \left(\frac{s}{2} + i\Delta h \tan(\theta)\right)^2} QY \left(1 - \frac{\sqrt{(i\Delta h)^2 - \left(\frac{d}{2}\right)^2}}{i\Delta h}\right) \quad (8)$$

Figure 7 presents the expected emission intensity observed from a thin solution layer ( $\Delta h$ ) as a function of distance from the fiber tip for samples with different absorptions (we want to stress that in this case we are considering just sample absorption  $A = \varepsilon C i h$  that is measured for the total sample thickness,  $h$ ). For the first  $700 \mu\text{m}$ , the signal is not observed (excitation and emission circles do not overlap). After that, the measured intensity quickly increases, reaches maximum, and drops. This reflects an increase in overlapping cones area as the distance from the fiber increases. The maximum signal intensity clearly depends on sample absorption. The relative signal increases for absorbances up to about 0.5 (absorption in 1 cm path) and then drops as absorbance increases. One needs to remember that significant cones overlap happens at a distance much larger than the distance  $x$  at which the excitation light intensity is significantly attenuated by sample absorption. Also, as we increase the sample absorbance (concentration), the center of gravity for observed signal distribution shifts closer to the fiber tip. It is impossible to experimentally measure intensity from the given layer of a continuous sample to

confirm our simulations presented in figure 7. In practice, we can only measure the overall (total) intensity as it is emitted by the entire sample. The total signal

detected from a sample of a given absorbance is a simple sum of individual signals from all layers,  $FT = \sum_i \Delta F_i$ .

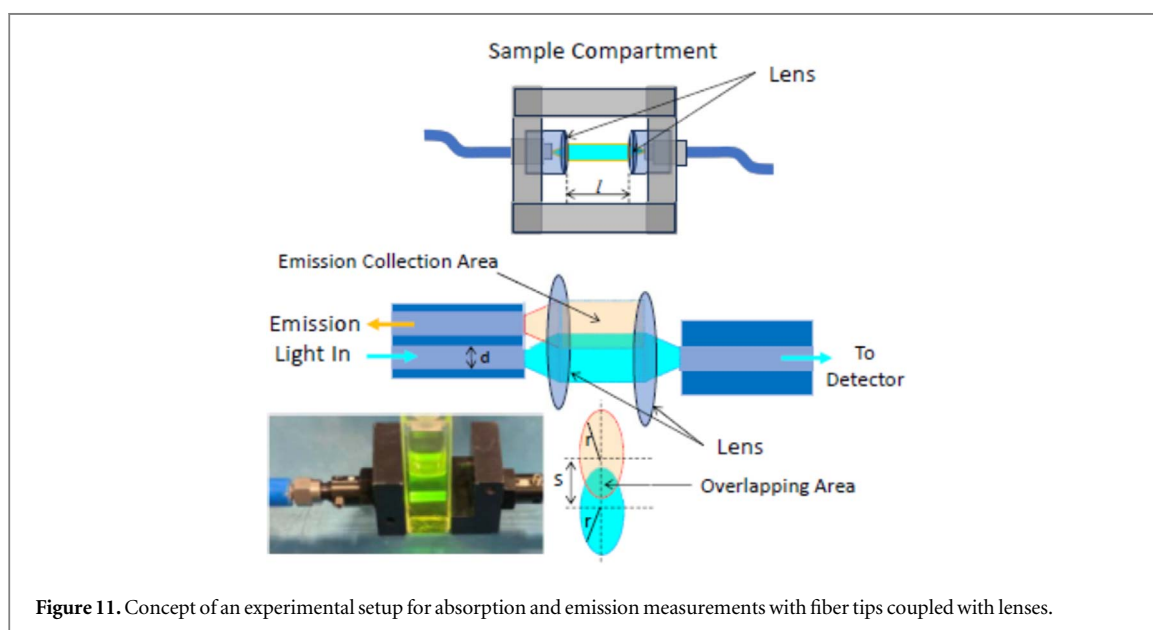
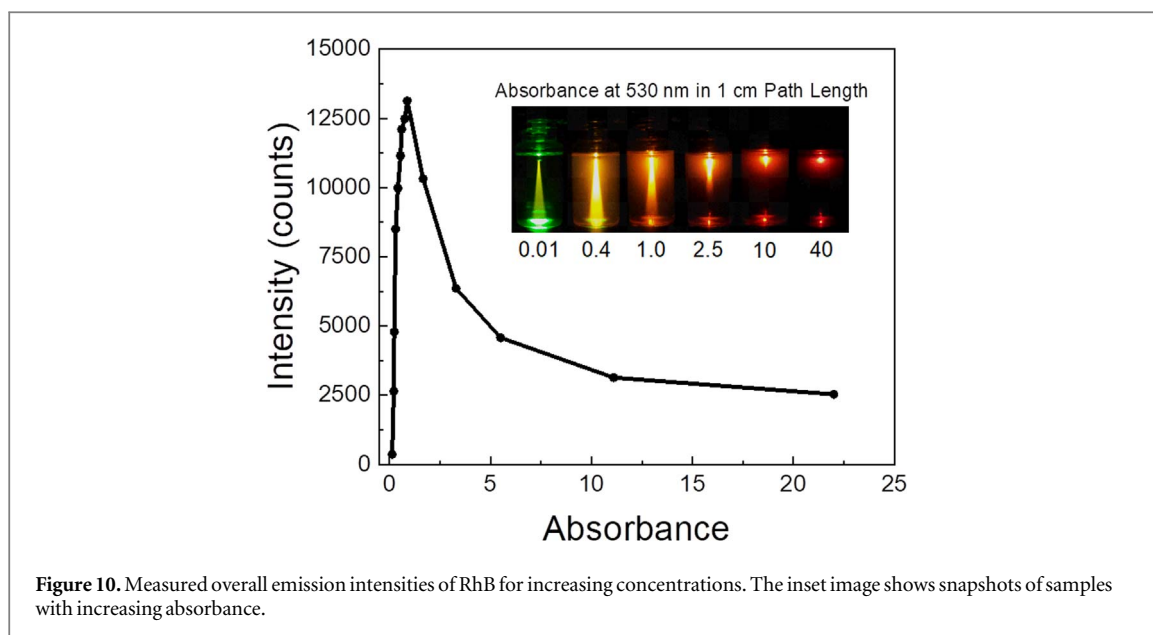
In figure 8, we present theoretical predictions for detected signals from solutions of increasing absorbance for 4 different separations between the fiber lines. For  $s = 0 \mu\text{m}$ , which represents a single line fiber, the observed intensity increases and asymptotically reaches a maximum for the highest absorbance. This is expected since, for high sample absorbance, most of the signal is generated close to the fiber tip, and the limit is just the number of photons available in the excitation beam. But already, for minimal separations  $s = 600 \mu\text{m}$  (two fiber lines of diameter  $600 \mu\text{m}$  for which the edges are in contact), we observe a quick signal increase that reaches a maximum at an absorbance of about 7 (absorption measured in a 1 cm path). In this case, the distance  $x$  for which excitation and emission cones start to overlap is practically zero. After the initial signal increases, the observed signal starts dropping. For higher absorptions, the excitation light does not sufficiently penetrate the solution to reach the full overlap of the cones, and the observed signal is



dominated by the closest layers for which the overlapping area is small. For higher separations of fiber lines,  $s$ , being 700, 900, and 1100  $\mu\text{m}$ , the maximum of detected signal shifts toward the smaller absorptions, and, for  $s = 900 \mu\text{m}$ , the maximum detected signal corresponds to an absorbance of about 1.5 in a 1 cm path. Also, when increasing the fiber lines separation, the overall detected signal drops significantly, especially when compared to a single fiber.

In figure 9, we present the measured emission spectra for Rhodamine B (RhB) solutions in EtOH excited at 530 nm. As we increase the concentration (absorbance), the observed signal at the emission maximum initially increases and reaches a maximum at an absorbance of 1.5 (absorption in 1 cm path). Then, the emission signal quickly drops with increasing concentrations. Furthermore, the maximum emission signal clearly red-shifts with increasing concentrations

of RhB due to the inner filter effect type II [24]. To verify our prediction in figure 8 experimentally, we use the emission signal observed for wavelengths over 580 nm, where the inner filter effect is not present (no spectral overlap). In figure 10, we present the measured signal as a function of RhB absorbance. The observed behavior is consistent with our predictions for a bifurcated fiber with a separation between lines  $s$  of about 900  $\mu\text{m}$ . The inset (photograph) in figure 10 shows an image of observed beam penetration for 6 different concentrations of RhB solutions. For low concentrations, the beam penetrates the entire bottle distance of about 6 cm, while for the highest concentrations, only the top part of the solution is penetrated by the excitation light. Also, the apparent color changes significantly from green (for lowest sample concentration) to red for high sample concentrations consistently with the observed spectral shift.

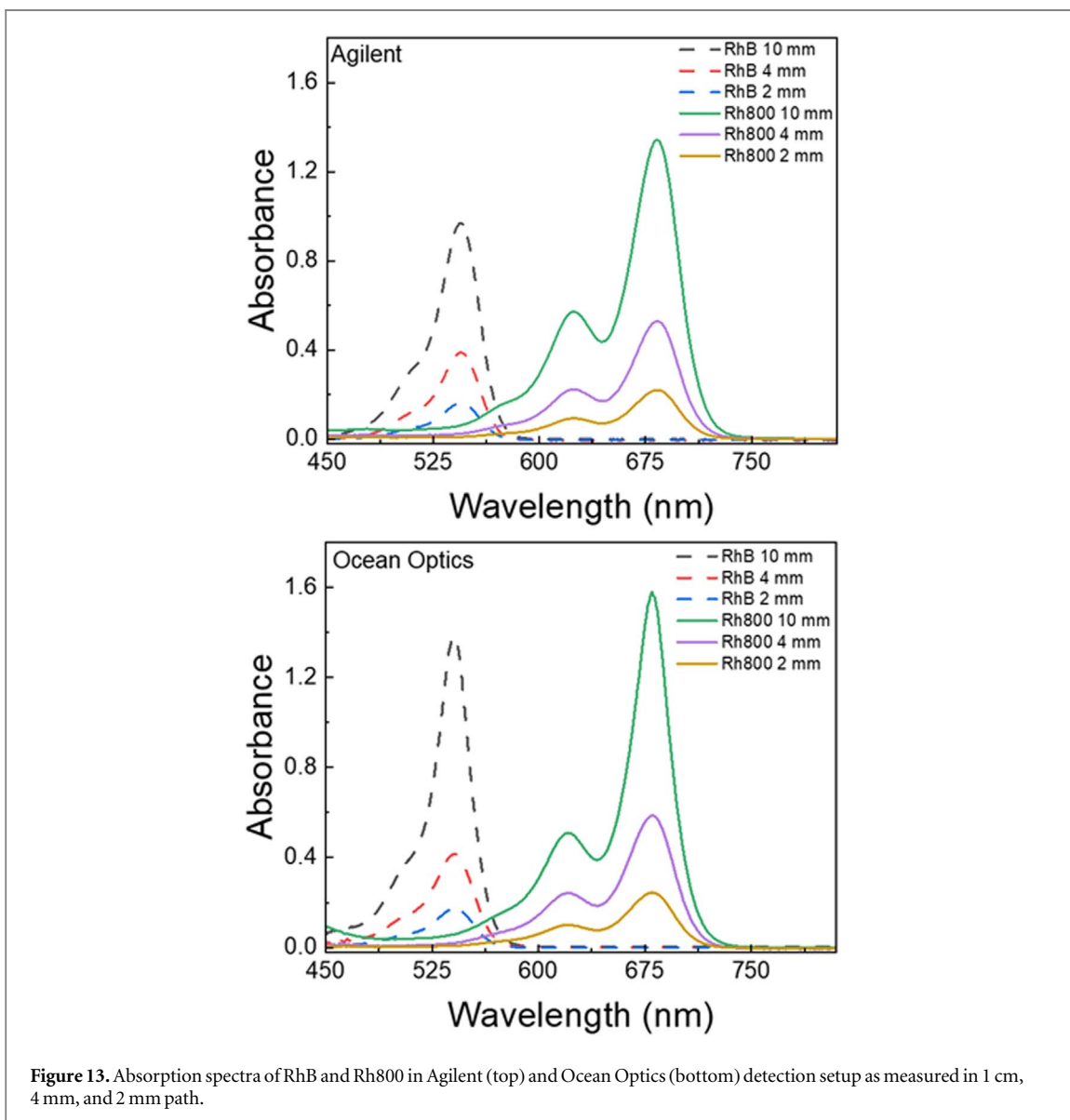
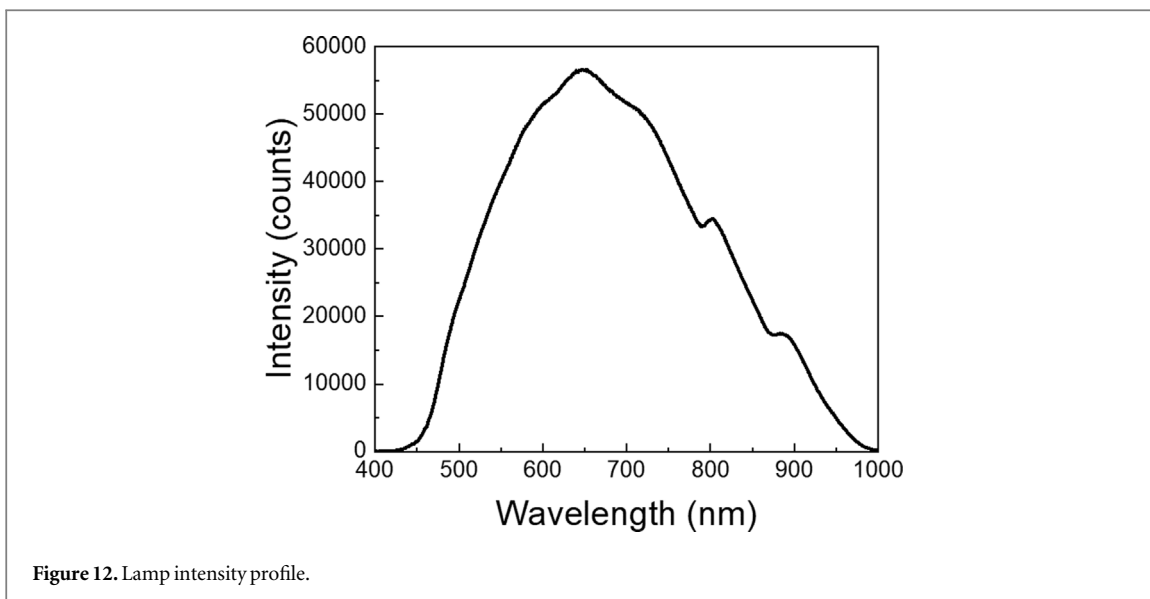


### 3. Bifurcated fiber with the collimating lens

One of the disadvantages of using a bare fiber is the difficulty of measuring sample absorption. For the separation distance in between two fibers facing against each other (light-delivering fiber and light-collecting fiber), distances larger than a few millimeters make the cone cross section much larger than the fiber's diameter, and the amount of collected light becomes insufficient. To limit the outward beam expansion and improve light collection from a larger area, light collimating elements (lenses) can be used. The concept for using collimated optics (lenses) is presented in figure 11. As the tip of the fiber-optic cable is positioned at the focal distance of the collimating lens, the emerging light forms a cylinder (parallel light beam). The overlapping area between two

cylinders (excitation cylinder - blue and observation cylinder - yellow) is now fixed (independent of distance). The overlapping surface of the excitation and collection cylinders depends on the separation distance of the different fibers and the focal distance of the lenses.

The important conceptual difference when compared to just a bare fiber tip is that the distribution of the excitation beam intensity is not dependent on distance from the fiber tip (more precisely, the distance from the surface of the lens). Proper alignment of the left and right fibers allows a large part of the delivered light to be collected by the opposite fiber and delivered to the detector. Effectively, sample absorbance and/or scattering are the only attenuating factors of the excitation beam intensity. Measuring the transmitted light intensity with just a reference solvent, followed by the



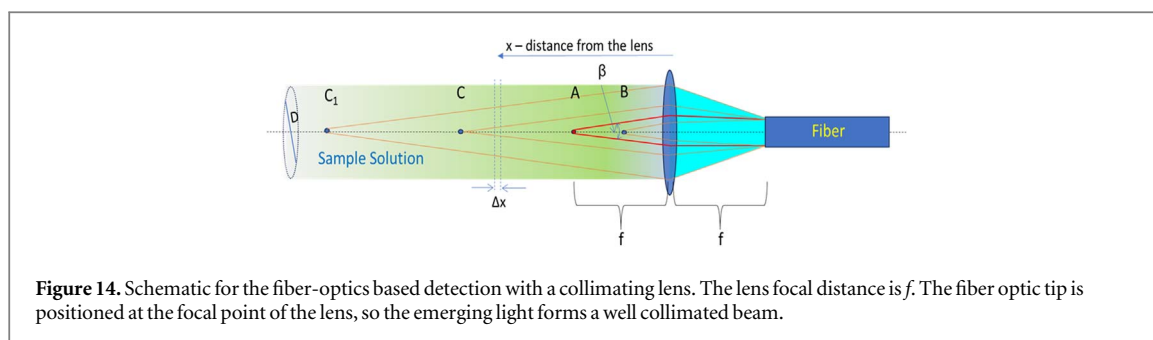


**Figure 14.** Schematic for the fiber-optics based detection with a collimating lens. The lens focal distance is  $f$ . The fiber optic tip is positioned at the focal point of the lens, so the emerging light forms a well collimated beam.

measurement of light intensity with the sample, allows us to calculate the sample absorption.

### 3.1. Absorbance measurements

To cover a large absorption range, we used two different dye concentrations and cuvette thicknesses of 10 mm, 4 mm, and 2 mm. The Ocean Optics detector only measures the light intensity of incoming light at different wavelengths. So, to calculate the absorbance, it is necessary to measure the light intensity detected with the cuvette filled with solvent (EtOH),  $I_R(\lambda)$ , and light intensity with the cuvette filled with the solution of the dye,  $I_S(\lambda)$ . The absorbance can then be calculated as:

$$A(\lambda) = -\log\left(\frac{I_S(\lambda)}{I_R(\lambda)}\right) \quad (9)$$

Using the configuration presented in figure 11, absorption measurements of Rhodamine 800 (Rh800) and RhB were obtained. As the source of light, we used the portable lamp from Ocean Optics with an intensity distribution from 450 to 900 nm, as shown in figure 12.

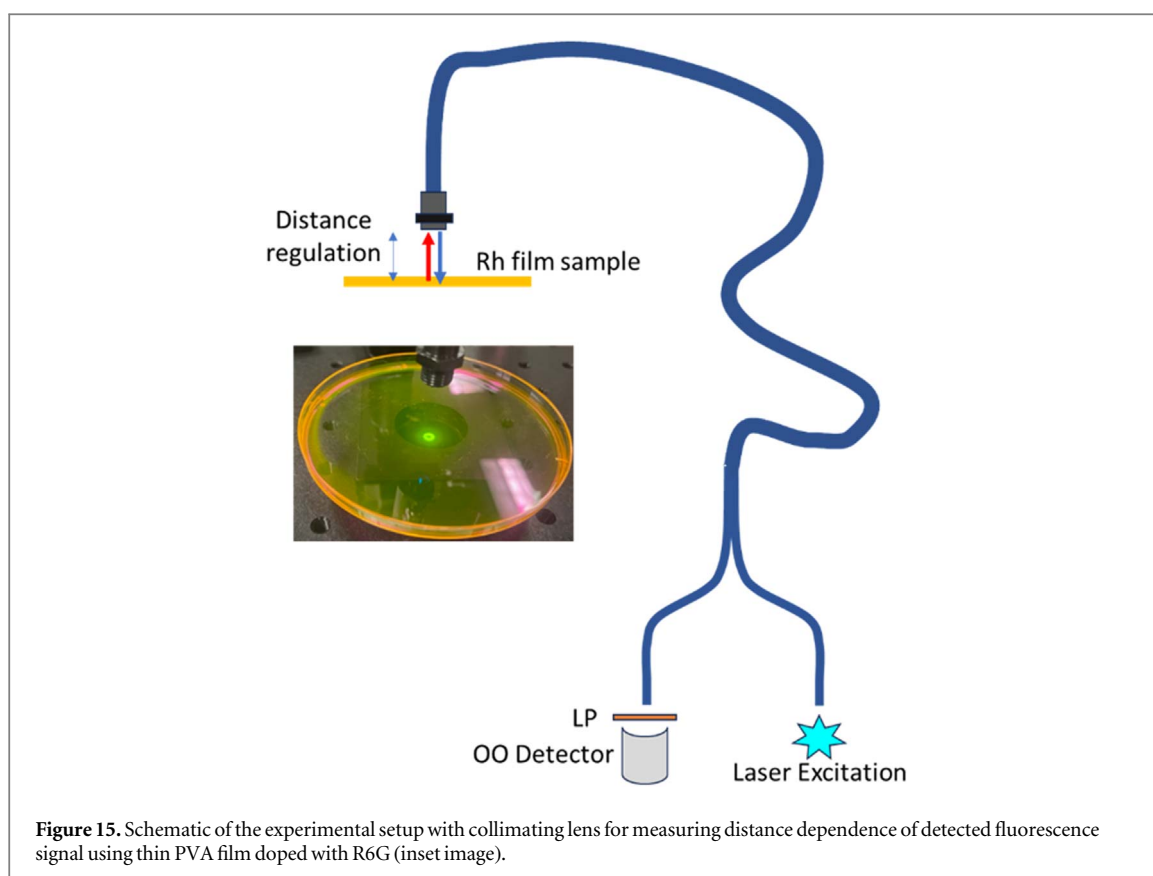
The absorption spectra of Rh800 and RhB are significantly different within the light range supplied by the lamp.

Figure 13 shows the absorption spectra (for Rh800—solid lines and RhB—dashed lines) measured in the Agilent spectrophotometer (top) and measured and calculated from the Ocean Optics detector (bottom). Solution of Rh800 and RhB in EtOH presenting absorbance of about 1.4 and 1 respectively were measured in 1 cm, 4 mm, and 2 mm path cuvettes. The Ocean Optics absorption spectra correspond well in the broad absorption range up to 1.5 with comparable noise. However, at higher absorption values (above 1), the intensity of transmitted light through the sample is highly attenuated (over 10 folds), and the Ocean Optics detector sensitivity/response becomes non-linear, compromising the detector sensitivity. However, using a fiber configuration, absorption spectrum for reasonably high maximum absorbance can easily be measured, but absorbance higher than 1.5 suffers signal deterioration when using an Ocean Optics detector.

### 3.2. Emission measurements

The bifurcated fiber equipped with a collimating lens forms a uniform parallel beam. This makes it possible to measure the absorption of solutions of significant (centimeter) thickness. In addition, emission measurements can be done simultaneously or in a quick sequential approach through the second line of bifurcated fiber. As presented in figure 11, the emission-collecting fiber-optic line will only detect signals from the overlapping area of two cylinders (excitation cylinder and collection cylinder). The overlapping area is described by equation (1) and is constant along the cylinders. To calculate the emission detected by the fiber equipped with a collimating lens, consider the schematic presented in figure 14.

The fiber-optic tip (end) is positioned at the focal point of the lens, so the light forms a well-collimated beam after passing through the lens. We assume that the geometrical parameters for cylinder collecting emission are equivalent to the cylinder formed by excitation light. The excitation and emission cylinders are just shifted by the fixed distance,  $s$ , as shown in figure 11. For the fiber-optics diameter much smaller than the lens diameter and focal distance,  $f$ , the quality of the emerging beam will be good, forming a simple cylinder, as shown in figure 14. In this case, the excitation efficiency will depend only on light attenuation due to the excitation beam's absorption and/or out-scattering. For samples with reasonable optical densities, the intensity will be inversely proportional to the distance and will decrease as the excitation beam penetrates the sample according to the Beer–Lambert law. For a sample that presents an absorbance of 1, the intensity at the end of the sample (left side in figure 14) decreases 10-fold compared to the initial intensity at the lens surface. The fluorescence light can be collected by the same fiber with a dichroic long-pass filter at the collection side, similar to the front-face geometry we discussed in [24]. Or it can be collected by the separate parallel fiber-optics line in a bifurcated (or coaxial) fiber for which the displacement/separation of a parallel fiber is significantly smaller than the lens diameter. For our considerations, we assumed a fiber size of 600  $\mu\text{m}$  and separation,  $s \sim 900 \mu\text{m}$  between centers of two lines, lens diameter of  $\sim 8 \text{ mm}$ , and focal distance of the lens is about 10 mm. Thus, we can



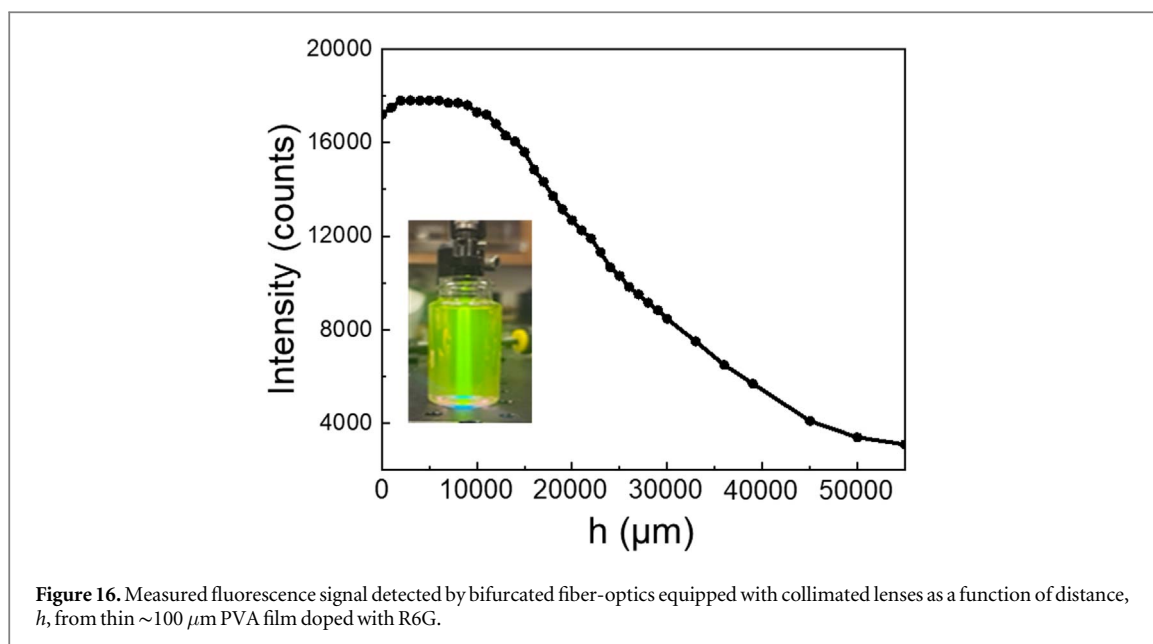
**Figure 15.** Schematic of the experimental setup with collimating lens for measuring distance dependence of detected fluorescence signal using thin PVA film doped with R6G (inset image).

assume that the displacement between delivering and collecting fibers is negligible. In this case, the excitation and collection cylinders are two parallel, partially overlapping cylinders displaced by the distance proportional to the displacement of the two fiber lines (for a single fiber line for excitation and emission collection, the displacement is 0).

To simplify our considerations, we discuss the fluorescence signal detected by the single fiber, as presented in figure 14. In the case of bifurcated fiber, the detected signal will be just scaled by the factor proportional to the overlapping areas of two cylinders. The detected signal is a product of excitation and emission collection efficiencies as a function of the distance from the lens. The intensity of excitation light changes as it penetrates the sample according to the Beer–Lambert law (equation (2)). The excited fluorophores emit uniformly/isotropically in space (fluorophore emits with equal probability in all directions—isotropic). In the case of the collecting lens, the efficiency (amount of collected emission signal from a given point) will depend on the distance from the lens that focuses the light into the fiber. For an emitting point at the focal distance (point A in figure 14), the amount of light that the lens will focus into the fiber will be the light emitted into the solid angle,  $\beta$ . The light emerging from a focal point after passing the lens forms a parallel beam to the optical axis, and all rays emitted at angles below the angle  $\beta$  (below thicker red ray marked in figure 14) will enter the fiber (all rays that are passing through the lens are parallel and are within the fiber’s diameter).

The diameter of the part of the lens that can collect emission light and focus it into the fiber is, in this case, equal to the diameter of the fiber that corresponds to a cylindrical angle  $\beta$  (figure 14). Any light coming at an angle larger than  $\beta$  will not be focused into the fiber. For points at a distance closer than the focal lens (like point B), the collection angle will be constant and equal to  $\beta$ . So, as we move closer to the lens, the surface area of the lens that can focus emission light into the fiber decreases proportionally to the distance squared ( $x^2$ ).

Effectively, the collection efficiency between the lens surface and focal point will be constant and will not depend significantly on the distance. The fraction of collected emission will be proportional to the ratio of the fiber tip surface ( $\frac{\pi d^2}{4}$ ) to the surface area of a sphere of radius equal to the focal distance  $f$  ( $\pi f^2$ ). For distances larger than the focal distance, such as points C and  $C_1$ , the collection angle should decrease. However, the active area of the lens focusing on the fiber will be increasing, partially compensating for the angle decrease. So, the efficiency for collecting the emission signal for points not much above the focal distance will have a slow decrease (slower than expected from quadratic distance dependence). For points beyond point  $C_1$ , the collection efficiency decreases proportionally to the distance squared. It is important to mention that these considerations are for points located along the optical axis. Although the efficiency for emission collection for points off the optical axis can be smaller, the



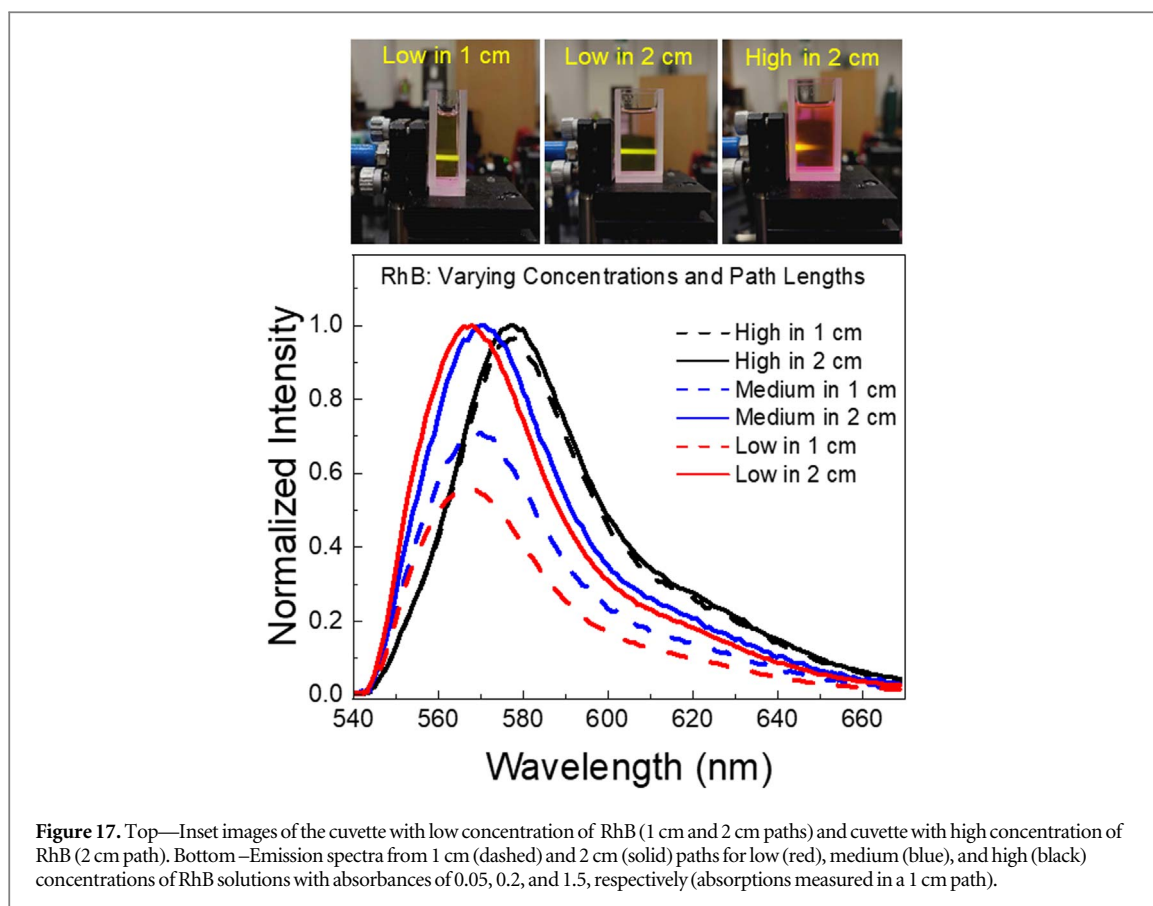
distance dependence should obey a general rule. There are a few conclusions resulting from the presented considerations. First, the signal detected from layers adjacent to the lens is not zero. Second, the observed intensity of the fluorescence signal should be independent of distance (constant) up to a lens focal distance. Third, the decrease of the signal for distances above focal distance should not be significant due to the increasing active area of the lens. The decrease for larger distances should be slower than the expected quadratic dependence found for the bare fiber tip.

To test our considerations experimentally, we used the experimental arrangement as shown in figure 15. We used the same thin PVA film doped with R6G. In figure 16, we present the measured emission signals from the R6G film as a function of the number of turns (distance from the film starting at direct contact). For the first 2–3 steps, the fluorescence signal slightly increases and then is constant for the next 20 steps. Effectively, for a distance of over 15 mm, the signal does not depend on the film separation. It is clear that within the focal distance, the signal is constant. Above the focal distance, the increase in distance is compensated by the increase in lens surface area utilized for collecting and effectively focusing the emission light into the fiber. Since the lens is mounted in a metal cast, the zero distance (contact point) is about 2 mm from the lens, making the effective distance for a constant signal over 15 mm. After the next 25 mm (50 turns), the signal drops only to 1/2. This clearly indicates that the signal drop does not obey a quadratic dependence, and the drop due to the distance increase is partially compensated by the increase of the apparent (utilized) surface of the lens (surface of the lens that can effectively focus light into the fiber tip).

We can conclude that when using a collimating lens, the detected signal in the first 15 mm is constant, and for the next 10–15 mm, the signal only moderately

depends on the distance from the lens. So, when using continuous samples (e.g., solutions) that have thicknesses below 15–20 mm, the detected emission signal for low optical density solutions will linearly depend on sample thickness. However, as we increase concentration (solution absorbance), the signal should not be linearly dependent on sample thickness.

To test these predictions, we used RhB solutions presenting absorbance from about 0.05 to 1.5 (as measured in a 1 cm path) in a 10 mm  $\times$  20 mm cuvette. The sample in such a cuvette can be switched easily (rotated) from a 1 cm to a 2 cm path. In figure 17, we present measured emission spectra of RhB solutions (absorbances of 0.05, 0.3, and 1.3) as measured along a 2 cm path (solid lines) and a 1 cm path (dashed lines). The presented spectra are normalized to the maximum measured in a long (2 cm) path. On the top of figure 17, we present 3 images that depict various measurements of the aforementioned set up. The left and middle image are of the low concentration solution in a 1 cm and 2 cm path, respectively. The right image is the measurement of the high concentration solution in the 2 cm path. For the lowest concentration (red lines), the emission signal measured in the 2 cm path is almost 2 times larger than that along the 1 cm path. Also, as seen in the images for both the 1 and 2 cm paths the fluorescence signal is uniform along the entire path and fluorescence appears green. For higher (medium) concentration (blue), the difference is only about 30% and for the highest concentration (black) the difference is minimal. As seen in inset images, the excitation beam barely penetrates the first half of the cuvette ( $\sim 1$  cm). Only a limited thickness is illuminated that contributes to the detected signal, independent of sample thickness. For low sample concentrations, the signal detected is linearly proportional to the thickness. When measuring samples from a limited distance of a few millimeters, the detected



signal will not depend significantly on the distance from the lens. This will allow many practical applications where the access to the sample is limited. For example, detecting fluorescence through the thick optical window of a bioreactor or detecting fluorescence from closed containers (e.g., bottles) for which we do not know transparent wall thickness and perturbation due to geometrical distance are impossible to account/correct for.

One important conclusion from measured emission spectra is that the detected emission spectrum clearly depends on sample concentration. As discussed by us [19, 21, 24], this is due to the secondary inner filter effect. This would be a significant hurdle in interpreting detected spectra of various solutions. So, developing a method to simply correct for the inner filter effect is necessary. However, we could not find such a method for fiber-based detection in literature. In Part II, we will present the original method to correct observed emission spectra for the inner filter effect.

Finally, we want to indicate that, for the bifurcated fiber, the maximum signal detected with the collimating lens is smaller (almost 3 times) than the maximum signal detected by the bare fiber at an optimal position. This is because the overlapping area is relatively small ( $\sim 30\%$ ) and does not increase/change with the distance like it is for cones observed for a bare fiber. This could be improved by decreasing the separation between fiber

lines, so for the single-line fiber it would be significantly better (100% overlap).

### 3.3. Conclusion

In this first tutorial we introduced the concept for using a simple optical fiber probe to measure fluorescence and absorption. The capability of simultaneous measurements of absorption and fluorescence from the sample opens the possibility to correct for inner filter effect type II and allow the recovery of the true emission spectrum of the sample. This will have significant implications for practical applications in industrial and biomedical settings.

### Funding

Funding provided by Novel Products Research of EMTEC is gratefully acknowledged. ZG acknowledges the support from 'Tex' Moncrief Jr.

### Data availability statement

The data cannot be made publicly available upon publication because they contain commercially sensitive information. The data that support the findings of this study are available upon reasonable request from the authors.

## ORCID iDs

Bong Lee  <https://orcid.org/0009-0003-7936-5327>  
Luca Ceresa  <https://orcid.org/0000-0001-8771-496X>  
Danh Pham  <https://orcid.org/0000-0003-0274-9640>  
Joseph Kimball  <https://orcid.org/0000-0001-5869-4883>  
Emma Alexander  <https://orcid.org/0000-0002-9226-2432>  
Xuan Ye  <https://orcid.org/0009-0004-8138-3425>

## References

- [1] Flusberg B, Cocker E, Piyawattanametha W, Jung J, Cheung E and Schnitzer M 2005 Fiber-optic fluorescence imaging *Nat. Methods* **2** 941–50
- [2] Gessei T, Arakawa T, Kudo H and Mitsubayashi K 2015 A fiber-optic sorbitol biosensor based on NADH fluorescence detection toward rapid diagnosis of diabetic complications *Analyst* **140** 6335–42
- [3] Kocincova A, Borisov S, Krause C and Wolfbeis O 2007 Fiber-optic microsensors for simultaneous sensing of oxygen and pH, and of oxygen and temperature *Anal. Chem.* **79** 8486–93
- [4] Rogers K and Poziomek E 1996 Fiber optic sensors for environmental monitoring *Chemosphere* **33** 1151–74
- [5] Shim M, Wilson B, Marple E and Wach M 1999 Study of fiber-optic probes for *in vivo* medical Raman spectroscopy *Appl. Spectrosc.* **53** 619–27
- [6] Tiangco C, Fon D, Sardesai N, Kostov Y, Sevilla F III, Rao G and Tolosa L 2017 Fiber optic biosensor for transdermal glucose based on the glucose binding protein *Sensors Actuators B* **242** 569–76
- [7] Wang X and Wolfbeis O 2016 Fiber-optic chemical sensors and biosensors (2013–2015) *Anal. Chem.* **88** 203–27
- [8] Wen-xu L and Jian C 2003 Continuous monitoring of adriamycin *in vivo* using fiber optic-based fluorescence chemical sensor *Anal. Chem.* **75** 1458–62
- [9] Yin M, Gu B, An Q, Yang C, Guan Y and Yong K 2018 Recent development of fiber-optic chemical sensors and biosensors: Mechanisms, materials, micro/nano-fabrications and applications *Coord. Chem. Rev.* **376** 348–92
- [10] Zhang X, Guo C, Li Z, Shen G and Yu R 2002 An optical fiber chemical sensor for mercury ions based on a porphyrin dimer *Anal. Chem.* **74** 821–5
- [11] Rosenberg M, Laursen B, Frankær C and Sørensen T 2018 A fluorescence intensity ratiometric fiber optics-based chemical sensor for monitoring pH *Adv. Mater. Technol.* **3** 1800205
- [12] Wang X-D and Wolfbeis O S 2013 Fiber-optic chemical sensors and biosensors (2008–2012) *Anal. Chem.* **85** 487–508
- [13] Wang X-d and Wolfbeis O S 2019 Fiber-optic chemical sensors and biosensors (2015–2019) *Anal. Chem.* **92** 397–430
- [14] Wolfbeis O S 2000 Fiber-optic chemical sensors and biosensors *Anal. Chem.* **72** 81–90
- [15] Wolfbeis O S 2006 Fiber-optic chemical sensors and biosensors *Anal. Chem.* **78** 3859–74
- [16] Bunting U, Lewitzka F and Karlitschek P 1999 Mathematical model of a laser-induced fluorescence fiber-optic sensor head for trace detection of pollutants in soil *Appl. Spectrosc.* **53** 49–56
- [17] Cooney T, Skinner H and Angel S M 1996 Comparative study of some fiber-optic remote Raman probe designs. Part I: model for liquids and transparent solids *Appl. Spectrosc.* **50** 836–48
- [18] Ma J, Chiniforooshan Y, Hao W, Bock W and Wang Z 2012 Easily fabricated, robust fiber-optic probe for weak fluorescence detection: modeling and initial experimental evaluation *Opt. Express* **20** 4805–11
- [19] Gryczynski Z and Gryczynski I 2019 *Practical Fluorescence Spectroscopy* (CRC Press, Taylor & Francis Group)
- [20] Jameson D 2014 *Introduction to Fluorescence* (CRC Press, Taylor & Francis Group)
- [21] Kimball J, Chavez J, Ceresa L, Kitchner E, Nurekeyev Z, Doan H, Szabelski M, Borejdo J, Gryczynski I and Gryczynski Z 2020 On the origin and correction for inner filter effects in fluorescence Part I: Primary inner filter effect-the proper approach for sample absorbance correction *Methods. Appl. Fluoresc.* **8** 033002
- [22] Lakowicz J 2006 *Principles of Fluorescence Spectroscopy* (Springer)
- [23] Valeur B and Berberan-Santos M 2012 *Molecular Fluorescence: Principles and Applications* (Wiley-VCH)
- [24] Ceresa L, Kimball J, Chavez J, Kitchner E, Nurekeyev Z, Doan H, Borejdo J, Gryczynski I and Gryczynski Z 2021 On the origin and correction for inner filter effects in fluorescence. Part II: Secondary inner filter effect-the proper use of front-face configuration for highly absorbing and scattering samples *Methods. Appl. Fluoresc.* **9** 035005